IOPscience iopscience.iop.org

Home Search Collections Journals About Contact us My IOPscience

Monte Carlo studies on the hadronic component of extensive air showers

This article has been downloaded from IOPscience. Please scroll down to see the full text article.

1969 J. Phys. A: Gen. Phys. 2 341

(http://iopscience.iop.org/0022-3689/2/3/014)

View the table of contents for this issue, or go to the journal homepage for more

Download details:
IP Address: 129.252.86.83
The article was downloaded on 31/05/2010 at 16:17

Please note that terms and conditions apply.

J. PHYS. A (GEN. PHYS.), 1969, SER. 2, VOL. 2. PRINTED IN GREAT BRITAIN

Monte Carlo studies on the hadronic component of extensive air showers

K. O. THIELHEIM and R. BEIERSDORF

Institut für Reine und Angewandte Kernphysik, Universität Kiel, Kiel, West Germany

MS. received 2nd October 1968

Abstract. Three-dimensional Monte Carlo calculations have been performed on the development of the hadronic component of extensive air showers using a semi-empirical model of high-energy nuclear interactions. Results include integral energy spectra and lateral distribution of nuclear active particles as well as total hadronic energy flux. The probability of multi-core showers is discussed. The contribution of pionization tends to mask the dependence of this probability on primary atomic number. Fluctuations of total and central hadronic energy flux are investigated. Maps of hadronic energy flux in the core region of individual showers are presented.

1. Introduction

Investigations of two different aspects of extensive air showers are performed. One is the astrophysical aspect, which is concerned with the combined distribution function of primary energy, mass number and direction, which constitutes the initial conditions of air shower development in the atmosphere. The other is the high-energy aspect, which is concerned with parameters describing the properties of strong interactions of extremely high energy in inelastic nucleon–nucleus and pion–nucleus interaction. The most direct access to such characteristics is expected in the observation of the hadronic component, which, unfortunately, constitutes less than one per cent of total particle number within an air shower. The rather complicated nature of cascade processes occurring in extensive air showers requires multi-parametric measurements as well as detailed theoretical investigations (Thielheim 1965).

The greater part of experimental effort has been devoted to mean characteristics of specified classes of extensive air showers at sea level, e.g. the integral energy spectrum of hadrons in showers of given size (Dovzenko *et al.* 1960, Vernov *et al.* 1960, Tanahashi 1965, Kameda *et al.* 1966, Hasegawa *et al.* 1966, Chatterjee *et al.* 1968, Böhm *et al.* 1968), lateral particle distribution (Kameda *et al.* 1966, Hasegawa *et al.* 1966, Chatterjee *et al.* 1968) and total energy flux (Tanahashi *et al.* 1965, Hasegawa *et al.* 1966, Chatterjee *et al.* 1968). Typical experiments of this type consist of detector arrangements which are shielded by layers of materials with high atomic number, such as lead or iron, to absorb the electromagnetic component. The energy flux in the hadronic component is estimated through conversion into electrons via pion production and neutral pion decay.

Investigations on the structure of the hadronic component in the core region of extensive air showers have become possible through the development of detector arrangements combining a large sensitive area with a rather high lateral resolution, such as the Sidney arrangement of 64 shielded scintillators covering a total area of 16 m^2 (Winn *et al.* 1965) or similar arrangements at mountain altitude (Miyake *et al.* 1966). Similarly, neon hodoscopes frequently used as electron detectors (Fukui 1961, Oda and Tanaka 1961, Thielheim 1964, Bagge *et al.* 1966) may be applied in experiments on high-energy hadrons under thick layers of material (Böhm *et al.* 1968). Characteristic features of the hadronic core structure are nuclear active multicores, which may be discussed either in terms of significant maxima of hadronic energy flux or in terms of single high-energy hadrons.

The interpretation of experimental results of extensive air showers meet with some characteristic difficulties, some of which are introduced by drawing conclusions about the mean behaviour of showers from the observation of very small samples owing to the

limitations of sensitive detector area. Further difficulties originate from the misinterpretation of secondary effects in particle detectors.

The diffusion theoretical approach and related methods are no longer sufficient in air shower theory. Comprehensive and systematic Monte Carlo studies, which have been performed first by Bradt *et al.* (1966) and by Thielheim and Karius (1966), have found wide application. Some authors have performed calculations which consist partly of Monte Carlo techniques and partly of semi-analytic methods (Tanahashi 1965, de Beer *et al.* 1966, Murthy 1967). Calculations which are purely Monte Carlo procedures, including a relatively large number of random variables corresponding to parameters of the underlying interaction model, are presented in this paper.

So far, there is no generally accepted theory of high-energy strong interactions. Therefore, the model is based partly on theoretical arguments and partly on empirical results obtained in the accelerator and emulsion range. The extrapolation of the latter data into the energy range covered by interactions occurring in extensive air showers is based on arguments considering an asymptotic behaviour of some of the differential cross sections and other characteristics of nuclear interactions. Obviously, there is still room for variation of such interaction parameters and one has therefore to distinguish conclusions derived from parametric studies which are strongly model dependent from those which are not. Some of the conclusions proposed below belong to the latter type.

2. Details of the calculation

(i) The relation between density and height in the atmosphere used in our calculations is based on empirical data (Kallmann-Bijl *et al.* 1961). Vertical incidence of the primary particles is assumed. Mean free paths are $\lambda_N = 80$ g cm^{-2} for nucleons and $\lambda_\pi = 100$ g cm^{-2} for pions. A-induced showers of primary energy E_0 are simulated by superposition of A p-induced showers of primary energy E_0/A. This procedure has been shown to lead to a reasonable compromise between different fragmentation models (Thielheim *et al.* 1968).

(ii) The model of inelastic nucleon–nucleus and pion–nucleus collisions is a combination of the isobar model and the CKP model†, which are frequently used in discussions on air shower development. The following propositions of the isobar model, as well as those of the CKP model discussed below, are not intended to give a physical explanation for the pion production process. The features of the former have been introduced in order to take into account the appearance of single high-energy secondary pions observed in the emulsion range (Teucher *et al.* 1959, Akashi *et al.* 1962, Dobrotin *et al.* 1965 a, b Kazuno 1964, Peters 1962, 1965). In a nucleon–nucleus collision the surviving baryon is assumed to be formed in an excited state N* with probability W_{anr}, while in pion–nucleus collisions there is no excitation of the surviving pion. The results presented below are obtained with N* = Δ (1236) and $W_{anr} = 0{\cdot}75$. The three possible charge states of the pion emerging from the decay of the excited baryon states are assumed to appear with equal probability. The decay of the excited baryon state simulated by the Monte Carlo procedure is supposed to be isotropic in the rest frame. The resulting distribution of energy of excitation pions in the laboratory system is approximately constant in the range of 0–40 per cent of the energy of the excited baryon state, the latter value being the upper limit of pion energy. The distribution of the nucleon–nucleus inelasticity κ_B, defined with respect to the surviving baryon state (which may be the excited state or the ground state), is proportional to $\kappa_B \exp(-\kappa_B/\text{const.})$, with $\langle\kappa_B\rangle = 0{\cdot}33$. The resulting nucleon–nucleus elasticity η_N defined with respect to the emerging nucleon ground state has the mean value $\langle\eta_N\rangle = 0{\cdot}56$. The distribution of pion–nucleus elasticity η_π is proportional to $\eta\pi \exp(-\eta\pi/\text{const.})$ with $\langle\eta_\pi\rangle = 0{\cdot}20$. The distribution of transverse momentum of the surviving particle is proportional to $p_\perp \exp(-p_\perp/\text{const.})$ with $\langle p_{\perp_B}\rangle = 0{\cdot}55$ GeV/c for the excited baryon state and $\langle p_{\perp_N}\rangle = 0{\cdot}42$ GeV/c for the nucleon ground state, if there is no excitation, and $\langle p_{\perp_\pi}\rangle = 0{\cdot}33$ GeV/c for the surviving pions.

According to our model the majority of secondary pions are generated through the pionization process following the conjectures of the CKP model. In high-energy collisions

† G. Cocconi, L. J. Koester and D. H. Perkins 1961, unpublished.

with collision energy $E > 10^{11}$ ev pions belonging to the forward cone are supposed to have a distribution of longitudinal momentum $p_{\parallel} \propto \exp(-p_{\parallel}/\text{const.})$ in the laboratory system. The mean longitudinal momentum $\langle p_{\parallel} \rangle$ is determined from the collision energy E so that the mean multiplicity $\langle n \rangle$ of pionization pions in the forward cone is $\frac{1}{2}\langle n \rangle = 1{\cdot}15E^{1/4}$ (E in Gev). Pions belonging to the backward cone were found to contribute only about one per cent of hadronic energy flux in typical showers of primary energy $E_0 = 10^{15}$ ev; therefore pions from the backward cone may be neglected. In low-energy collisions with collision energy $E < 10^{11}$ ev, where the forward and backward cones are no longer strictly separated, the distribution of longitudinal momentum in the high-energy tail of secondary pions is described by the function given above with $\langle p_{\parallel} \rangle$ adjusted such as to give the contribution $1{\cdot}4E^{1/4}$ to the mean multiplicity of pionization pions.

The distribution of transverse momenta is proportional to $p_{\perp_\pi} \exp(-p_{\perp_\pi}/\text{const.})$ for pionization pions, with $\langle p_{\perp_\pi} \rangle = 0{\cdot}33$ Gev/c independent of collision energy.

Different charge states of pions are determined by the Monte Carlo procedure assuming equal probability for each of them.

(iii) Results presented in this paper are based on three-dimensional Monte Carlo simulations of the nuclear active component of one set of 168 p-induced showers of primary energy $6{\cdot}25 \times 10^{13}$ ev and three sets of 100 p-induced showers of primary energy $2{\cdot}5 \times 10^{14}$ ev, 10^{15} ev and 4×10^{15} ev, respectively. The three sets of p-induced showers of lower primary energy have been used to construct sets of A-induced showers of primary energy 4×10^{15} ev comprising 25 α-induced showers, 6 ^{16}O-induced showers and 2 ^{64}Cu-induced showers.

A set of data is obtained for each individual shower, from which besides other information a matrix of 50×50 elements is prepared giving the logarithm (base 10) of the energy flux in squares of 10×10 cm^2 each, covering a total area of 5×5 m^2, the centre of which coincides with the shower axis.

Results are discussed in terms of the mean combined distribution $2\pi r f_{A,E_0}(E, r)$ of hadron energy E and distance r from the shower axis and in terms of the probability $P_{A,E_0}(\geq E, D)$ per shower to have at least two hadrons with energy greater than E at relative distance greater than D.

Additionally, 4 sets of 2500 p-induced showers each have been simulated at primary energies mentioned above, considering only the longitudinal development of hadrons with energy greater than 3×10^{12} ev. These results have been used to prepare the high-energy part of the integral energy spectrum presented in figure 2.

Besides data concerning nuclear active particles the total electron number N_e of each shower has been calculated for comparison with experimental data referring to shower size. Calculations have been performed using data obtained with approximation B of electromagnetic cascade theory (Thielheim and Siewers, to be published). Mean total electron numbers are shown in table 1 for various values of A and E_0 and may be represented approximately by $\langle N_e \rangle_{A,E_0} = 1{\cdot}23 \times 10^{-2} A^{-0{\cdot}2} E_0^{1{\cdot}2}$ (E_0 in Gev).

Table 1. Mean total electron number $\langle N_e \rangle$ of showers of primary energy $E_0 = 4 \times 10^{15}$ ev and primary mass numbers A = 1, 4, 16 and 64

A	N_e
1	$1{\cdot}04 \times 10^6$
4	$7{\cdot}72 \times 10^5$
16	$6{\cdot}22 \times 10^5$
64	$4{\cdot}86 \times 10^5$

3. Mean properties of hadrons at sea level

(i) The mean total energy flux

$$\langle E_{\text{tot}} \rangle_{A,E_0} = \int_{10^{10}\text{ ev}}^{\infty} \mathrm{d}E \int_0^{\infty} 2\pi r \, \mathrm{d}r \, E f(E, r)$$

of hadrons in A-induced showers of primary energy E_0 at sea level is presented in figure 1.

This result may be represented in the form

$$\langle E_{\text{tot}} \rangle_{A,E_0} = 1{\cdot}35 \times 10^{-3} A^{-0{\cdot}2} E_0^{1{\cdot}2} \, (E_0 \text{ in GeV})$$

which is presented in figure 1. As was mentioned in the preceding section (table 1), the same dependence on primary energy and primary mass number is obtained for the mean total electron number.

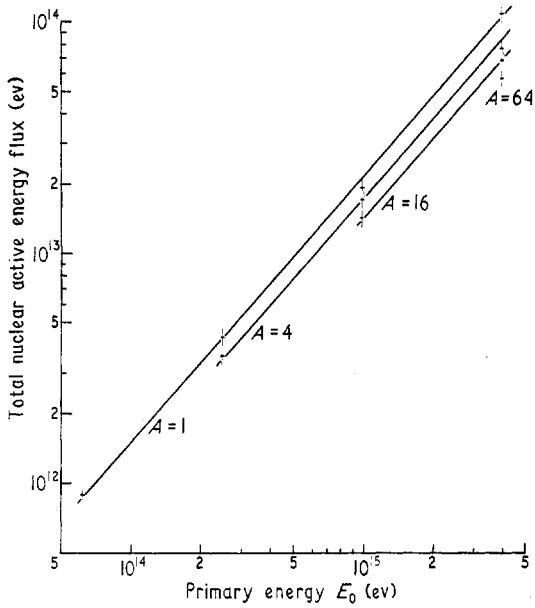

Figure 1. Mean total energy flux of nuclear active particles $\langle E_{\text{tot}} \rangle$ as a function of primary energy E_0 for various primary mass numbers A.

Therefore, the ratio $\langle E_{\text{tot}} \rangle_{A,E_0} / \langle N_e \rangle_{A,E_0} = (1{\cdot}1 \pm 0{\cdot}2) 10^8$ ev is independent of A and E_0 in a wide range of primary mass number and energy. One may suspect that this ratio is rather insensitive to special features of nuclear interaction models. Thus, Bradt and Rappaport (1968) obtained $\langle E_{\text{tot}} \rangle_{A,E_0} / \langle N_e \rangle_{A,E_0} = 10^8$ ev from Monte Carlo calculations resulting in values of $\langle E_{\text{tot}} \rangle_{A,E_0}$ and $\langle N_e \rangle_{A,E_0}$ which are smaller by a factor of 2·5 than our values at the same primary energy. Measurements of Tanahashi (1966) resulted in

$$\frac{\langle E_{\text{tot}} \rangle_{A,E_0}}{\langle N_e \rangle_{A,E_0}} = (0{\cdot}85 \pm 0{\cdot}3) 10^8 \text{ ev}.$$

(ii) The integral energy spectrum $\int_E^\infty \mathrm{d}E \int_0^\infty \mathrm{d}r \, 2\pi r f(E, r)$ is presented in figure 2. In the range of energy 10^{11} ev $\lesssim E \lesssim E_0/20A$ it may be represented by a power law, which is most obvious for p-induced showers, where the exponent is $-1{\cdot}21$. At lower energies the spectrum flattens, owing to increasing decay probability of pions. At higher energies the spectrum steepens, as a consequence of finite primary energy. The existence of a range which is governed by a power law may be understood as an indication of a state of equilibrium in nuclear active cascade development. Theoretical values of exponent given by other authors are $-1{\cdot}0$ (Bradt and Rappaport 1968) and $-1{\cdot}1$ (Murthy 1967). Measurements resulted in $-1{\cdot}08$ to $-1{\cdot}19$ (Chatterjee *et al.* 1968), $-1{\cdot}2$ (Tanahashi 1965), $-0{\cdot}8$ to $-1{\cdot}3$ (Vernov *et al.* 1960) and $-1{\cdot}2$ (Böhm *et al.* 1968). Absolute values of the integral energy spectrum at fixed primary energy depend strongly on nuclear interaction parameters, especially on mean nucleon–nucleus elasticity. Consequently, Bradt and Rappaport (1968), using $\langle \eta_N \rangle = 0{\cdot}5$, found spectra which are lower than ours by a factor of about 4. But good agreement is obtained when the spectra are normalized to the same shower sizes (Bradt and Rappaport 1968, Tanahashi 1965).

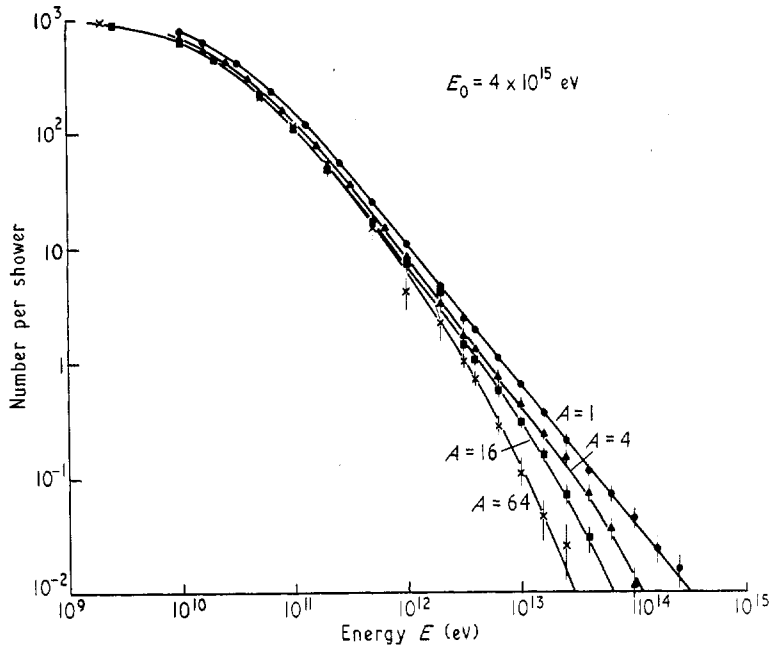

Figure 2. Integral energy spectrum of nuclear active particles for showers of primary energy $E_0 = 4 \times 10^{15}$ ev and primary mass numbers $A = 1$, 4, 16 and 64.

(iii) The lateral distribution $\int_E^\infty dE\, f(E, r)$ is shown in figure 3 for $E = 10^{10}$ ev and in table 2 for $E = 10^{10}$ ev, $E = 10^{11}$ ev and $E = 10^{12}$ ev for A-induced showers of primary

Table 2. Nuclear active particle density $n(r)$ (m^{-2}) of showers of primary energy $E_0 = 4 \times 10^{15}$ ev and primary mass numbers $A = 1$, 4, 16 and 64 for various values of distance r (m) from the shower axis and minimum energy E (eV) of nuclear active particles

$E_0 = 4 \times 10^{15}$ ev $\quad n(r) = \int_E^\infty dE f(E, r)$

	A \ r (m)	0·126	0·501	1·26	5·01	12·6	50·1	126
$E = 10^{11}$ ev	1	123	30	10·4	1·40	0·220	$3{\cdot}3 \times 10^{-3}$	5×10^{-5}
	4	90	26	8·5	1·13	0·20	$3{\cdot}2 \times 10^{-3}$	4×10^{-5}
	16	30	20	6·4	1·03	0·20	$3{\cdot}6 \times 10^{-3}$	(3×10^{-5})
	64	(16)	11	5·5	1·05	0·18	3×10^{-3}	(6×10^{-5})
$E = 10^{11}$ ev	1	$1{\cdot}0 \times 10^{2}$	17	4·1	0·21	$1{\cdot}2 \times 10^{-2}$	2×10^{-5}	—
	4	7×10^{1}	16	3·4	0·19	$1{\cdot}2 \times 10^{-2}$	3×10^{-5}	—
	16	2×10^{1}	13	2·8	0·15	1×10^{-2}	—	—
	64	—	4	3	0·2	2×10^{-2}	—	—
$E = 10^{12}$ ev	1	32	1·6	0·12	5×10^{-4}	—	—	—
	4	14	1·9	0·1	10^{-4}	—	—	—
	16	10^{1}	2	0·3	—	—	—	—
	64	—	(1)	(0·2)	—	—	—	—

energy 4×10^{15} ev. One may verify from figure 2 that spectra are flattening with increasing primary mass number A at distances less than about 3 m from the shower axis, as may be expected from the fact that the number of nuclear active particles of highest energies

decreases with increasing primary mass number at fixed primary energy. At distances greater than about 10 m from the shower axis the lateral distribution for different values of primary mass number A exhibit stronger convergence than one would expect from comparison of energy spectra presented in figure 2. This feature may be explained by detailed investigations on the combined distribution of energy and distance. Decrease of

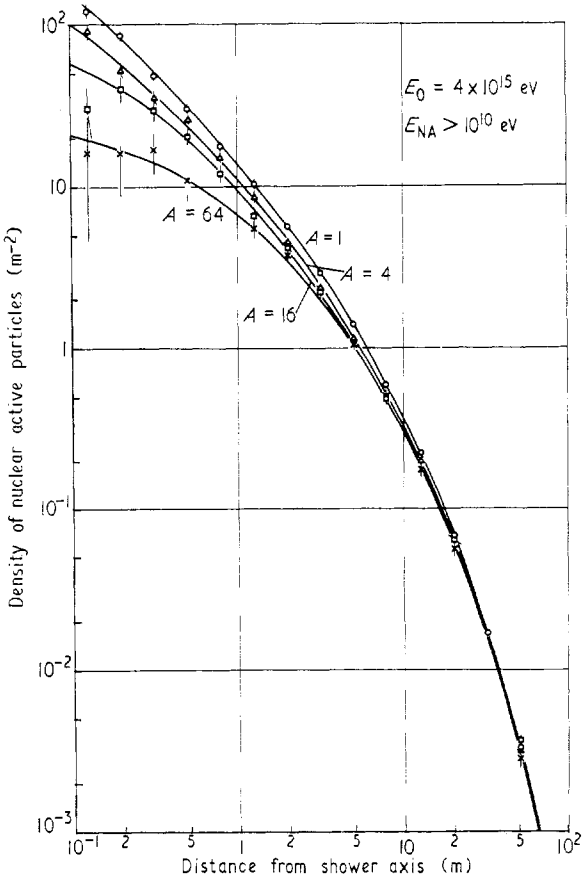

Figure 3. Lateral distribution of nuclear active particles for showers of primary energy $E_0 = 4 \times 10^{15}$ ev and primary mass numbers $A = 1$, 4, 16 and 64.

particle number with increasing A is compensated by increasing mean distance of particles from the shower axis (table 3) owing to the transition to greater heights of origin for particles of given energy E. The latter effect is more important than differences in the lateral diffusion due to different numbers of preceding interactions.

Table 3. Mean distance from the shower axis $\langle r \rangle$ (m) of nuclear active particles of energy E(eV) in showers of primary energy $E_0 = 4 \times 10^{15}$ eV and primary mass number A

$$\langle r \rangle = \int_0^\infty \mathrm{d}r\, r f(E, r) 2\pi r$$

E(ev)	$1{\cdot}12 \times 10^{10}$		$1{\cdot}12 \times 10^{11}$		$1{\cdot}12 \times 10^{12}$	
A	1	64	1	64	1	4
$\langle r \rangle$ (m)	19	21	4·9	8·0	0·65	0·85

There is a general agreement between the data presented above and those calculated by Bradt and Rappaport (1968) and Murthy (1967), while experimental results of Kameda *et al.* (1966), Hasegawa *et al.* (1966) and of the Bombay group (Chatterjee *et al.* 1968) indicate a flattening of lateral distribution with increasing size.

(iv) The probability per A-induced shower to have at least two nuclear active particles of energy greater than E, the distance of which exceeds D at sea level, is presented in figure 4(a) as a function of primary energy E_0. The upper and lower parts of this diagram

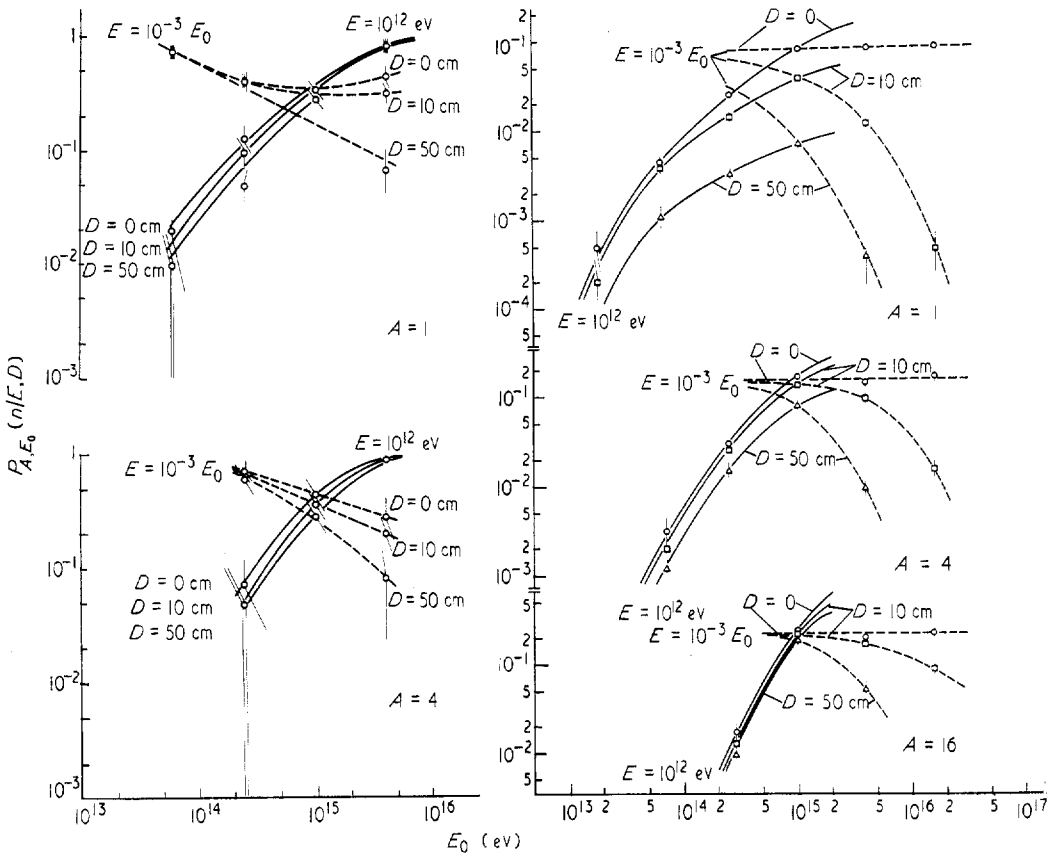

Figure 4. Probability $P_{A,E_0}(2/E, D)$ per A-induced shower of primary energy E_0 to have at least two nuclear active particles with relative distance greater than D and energy exceeding $E = 10^{12}$ ev (full lines) and $E = 10^{-3}E_0$ (broken lines) as a function of primary energy E_0. (a) All hadrons; (b) nucleons and excitation pions.

refer to p-induced and α-induced showers, respectively. Results are given for various values of D. Full lines correspond to fixed values of E, while broken lines were obtained with E proportional to E_0.

The same probability is presented in figure 5(a) as a function of primary mass number A for showers of primary energy $E_0 = 4\times10^{15}$ ev. The minimum energy of the particles is $E = 4\times10^{12}$ ev. As is obvious from this diagram, the probability of A-induced showers of given energy having nuclear active multicores is almost independent of primary mass number. Therefore, in these results there is no indication of the possibility of measuring primary mass composition through the observation of nuclear active multicore structure.

Former results (Thielheim and Karius 1966, Thielheim *et al.* 1968) showed that the contribution of the surviving baryon and of the pions from baryon excitation to the aforementioned probability exhibits a dependence on primary mass number. As one may conclude from our present calculations, the contribution of pions from pionization tends to

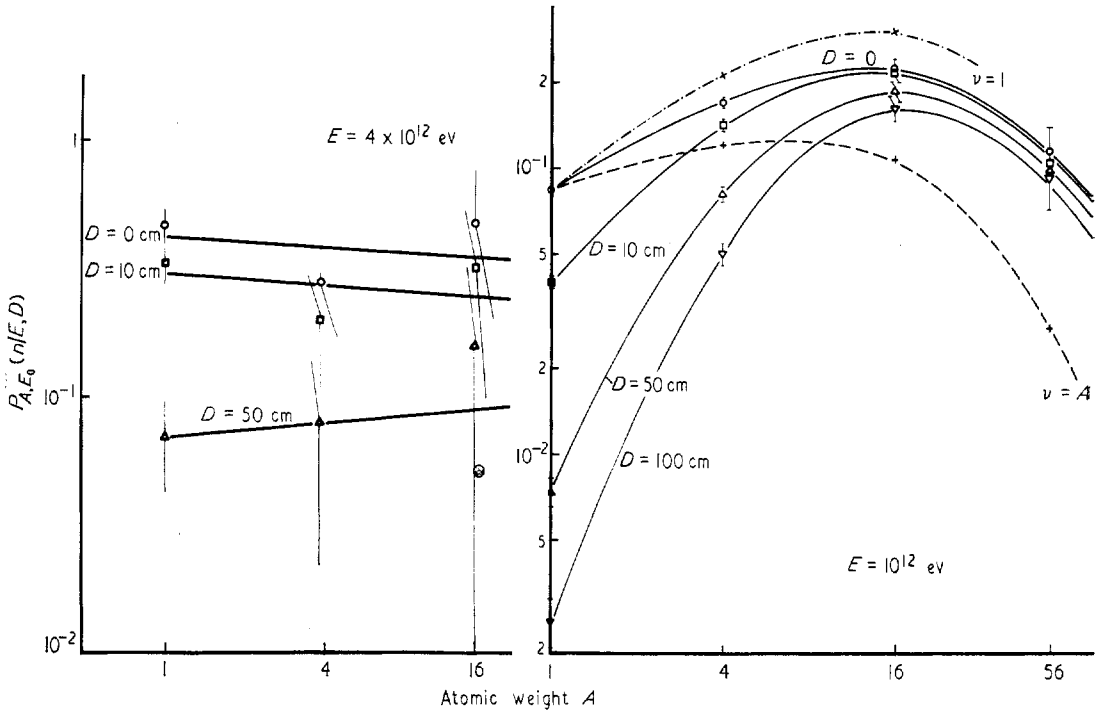

Figure 5. Probability $P_{A,E_0}(2/E, D)$ per A-induced shower of primary energy E_0 to have at least two nuclear active particles with relative distance greater than D and energy exceeding $E = 10^{-3}E_0$ as a function of primary mass number A. (*a*) All hadrons in showers of primary energy $E_0 = 4 \times 10^{15}$ ev; (*b*) nucleons and excitation pions in showers of primary energy $E_0 = 10^{15}$ ev. The broken lines indicate the influence of two other fragmentation models. ν is the number of nucleons out of the primary nucleus initiating meson production in the first collision.

mask this dependence and, therefore, to diminish the information on primary mass number contained in the high-energy part of the hadronic component of extensive air showers.

Thus, the results of our calculations do not confirm the possibility of interpreting the observed hadronic multicore structure of showers as being due to heavy primaries (Winn *et al.* 1965, Bray *et al.* 1966).

4. Fluctuations of the nuclear active component

(i) The combined distribution of total energy flux E_{tot} of hadrons and of total electron number N_e is presented in figure 6 for A-induced showers of primary energy 4×10^{15} ev. The total distributions of E_{tot} and N_e are given in the histograms on the left and below, respectively, for p-induced showers and α-induced showers, separately.

As has already been mentioned in the preceding section, there is a weak decrease of mean hadronic energy flux with increasing primary mass number at fixed primary energy. This dependence is masked by fluctuations of E_{tot}. Therefore, primary composition cannot be inferred from the observation of E_{tot}. As was mentioned before, the ratio of total hadronic energy flux to total electron number, $\langle E_{\text{tot}} \rangle_{A,E_0} / \langle N_e \rangle_{A,E_0}$, is independent of primary mass number and primary energy. But the fluctuations of this ratio differ widely for different values of primary mass number. As may be verified from an analogous diagram showing combined distributions for various values of primary energy, from which figure 6 has been constructed. Thus, owing to the aforementioned properties of the mean value and standard deviation the latter parameter may be discussed in investigations on primary mass composition.

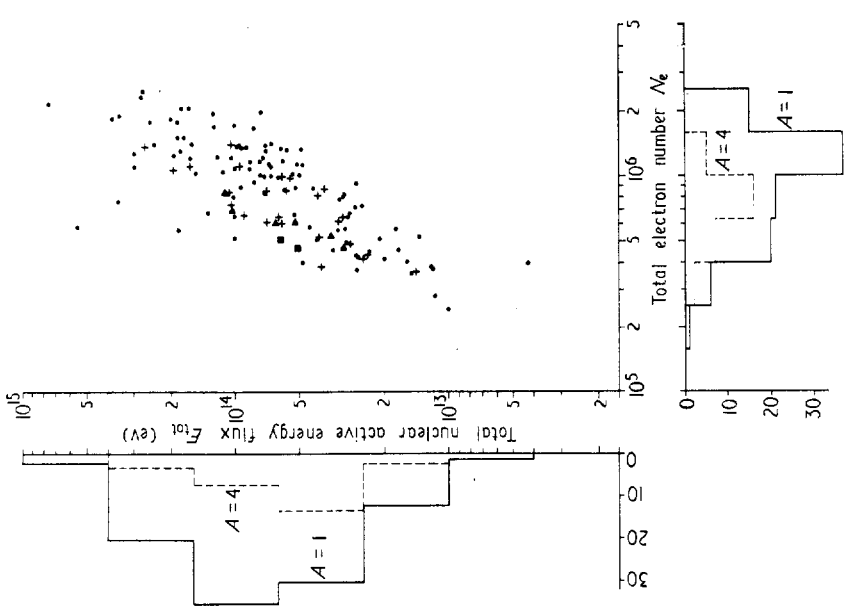

Figure 6. Combined distribution of total nuclear active energy flux E_{tot} and of total electron number N_e for A-induced showers of primary energy 4×10^{15} ev. Total distributions of E_{tot} and N_e are given in the histograms on the left and below, respectively, for p- and α-induced showers, separately. ● $A = 1$; + $A = 4$; ▲ $A = 16$; ■ $A = 64$.

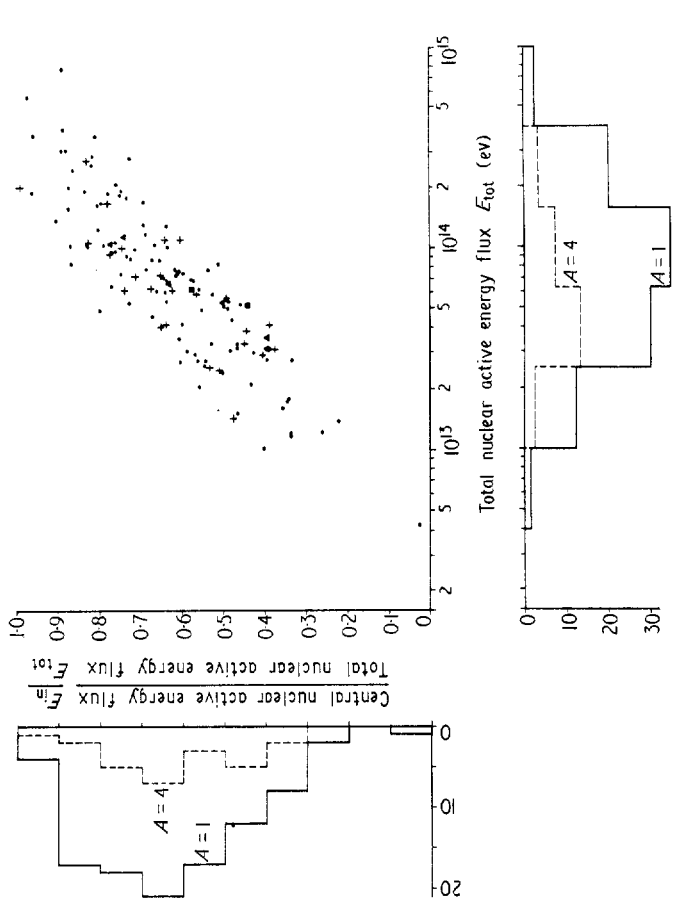

Figure 7. Combined distributions of ratio E_{in}/E_{tot} and of E_{tot}, where E_{in} is the nuclear active energy flux within a square of 5×5 m^2, the centre of which is given by the shower axis, and E_{tot} is the total nuclear active energy flux. Total distributions of E_{in}/E_{tot} and E_{tot} are given in the histograms on the left and below, respectively, for p- and α-induced showers, separately. ● $A = 1$; + $A = 4$; ▲ $A = 16$; ■ $A = 64$.

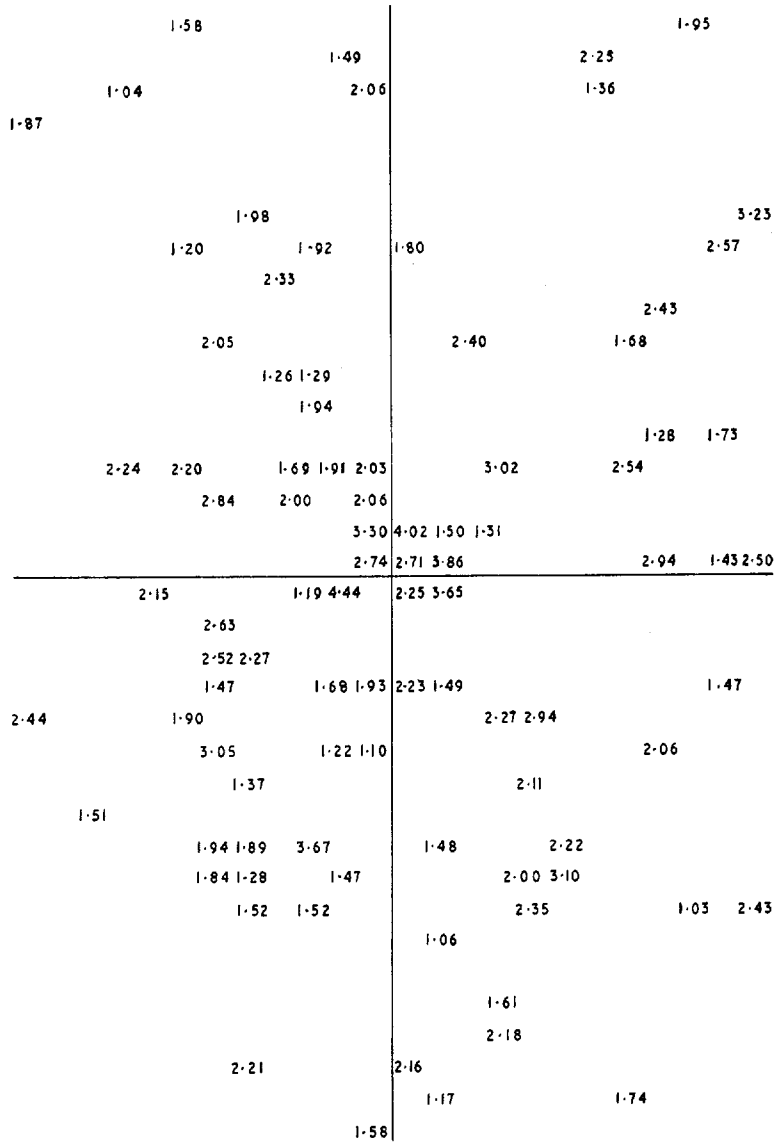

Figure 8. Map of hadronic energy flux within the core region of a p-induced shower of primary energy $E_0 = 4 \times 10^{15}$ ev. Elements are the logarithm of the energy flux (Gev) in squares of 10×10 cm^2. The centre of the map coincides with the shower axis. The central hadronic energy flux is rather typical, with $E_{1n} \simeq \langle E_{1n} \rangle_{A,E_0}$ for $A = 1$ and $E_0 = 4 \times 10^{15}$ ev.

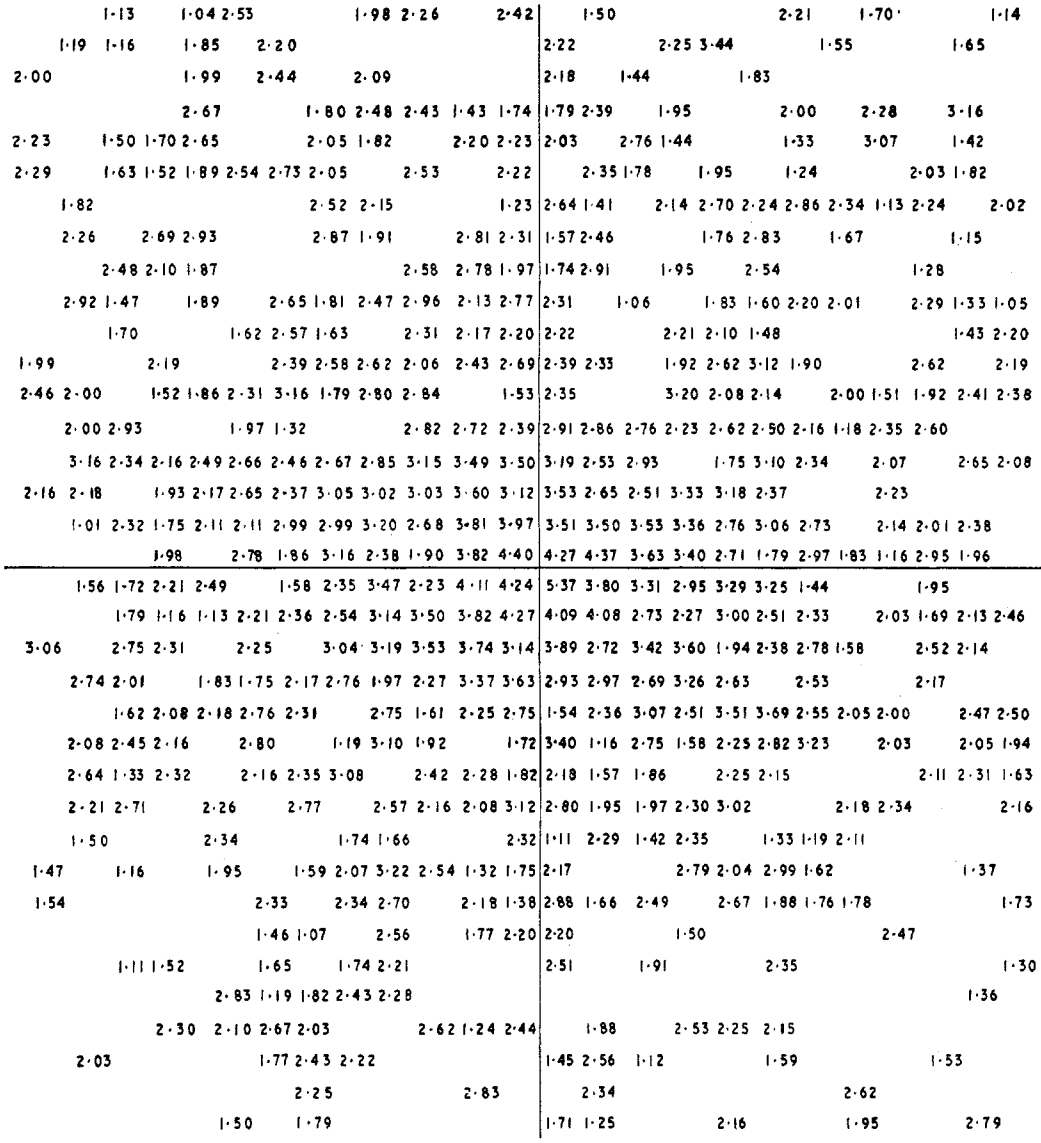

Figure 9. Map of the hadronic energy flux within the core region of a p-induced shower of primary energy $E_0 = 4 \times 10^{15}$ ev. Elements are the logarithm of the energy flux (GeV) in squares of 10×10 cm^2. The centre of the map coincides with the shower axis. This is the map for the shower with the highest central hadronic energy flux found in the calculated set of 100 p-induced showers of primary energy $E_0 = 4 \times 10^{15}$ ev.

(ii) The hadronic energy flux E_{in} within a square of 5×5 m^2, the centre of which is given by the shower axis, has been calculated for each Monte Carlo shower. The combined distribution of E_{in}/E_{tot} and E_{tot} is presented in figure 7, together with a histogram on the left showing the total distribution of E_{in}/E_{tot}.

Since the ratio E_{in}/E_{tot} reflects the concentration of hadrons near the shower axis, one may verify from this figure that there is a strong correlation between central and total hadronic energy flux. Fluctuations of E_{in} are found to be stronger than those of E_{tot}.

(iii) As an illustration of the hadronic core structure of extensive air showers, two maps are presented in figures 8 and 9, which give the distribution of energy flux within the core region of two showers taken from the set mentioned above. Elements are the logarithm of energy (GeV) per 10×10 cm^2. Both are p-induced showers of primary energy 4×10^{15} ev. The first one is rather typical with $E_{in} \simeq \langle E_{in} \rangle$ for this set of showers, while the second one exhibits the highest value of E_{in} found in this set. The one with the lowest value of E_{in}, which is also a p-induced shower, is not reproduced here, since there are only two elements greater than 1·00 within the total area of 5×5 m^2.

Acknowledgments

We wish to acknowledge financial support by the Deutsche Forschungsgemeinschaft and we wish to express our gratitude to the Deutsches Rechenzentrum in Darmstadt, where the computational work was done.

References

Akashi, M., *et al.*, 1962, *Int. Conf. on High-Energy Physics, CERN* (Geneva: IUPAP), pp. 633–6.

Bagge, E., *et al.*, 1966, *Proc. 9th Int. Conf. on Cosmic Rays, London*, 1965 (London: Institute of Physics and Physical Society), pp. 738–41.

de Beer, J. F., Holyoak, B., Wdowczyk, J., and Wolfendale, A. W., 1966, *Proc. Phys. Soc.*, **89**, 567–85.

Böhm, E., *et al.*, 1968, *Proc. 10th Int. Conf. on Cosmic Rays, Calgary*, 1967, Vol. 2 (Ottawa: National Research Council of Canada), pp. 50–5.

Bradt, H., La Pointe, M., and Rappaport, S., 1966, *Proc. 9th Int. Conf. on Cosmic Rays, London*, 1965 (London: Institute of Physics and Physical Society), pp. 651–65.

Bradt, H., and Rappaport, S., 1968, *Phys. Rev.*, **164**, 1567–83.

Bray, A. D., *et al.*, 1966, *Proc. 9th Int. Conf. on Cosmic Rays, London*, 1965 (London: Institute of Physics and Physical Society), pp. 68–71.

Chatterjee, B. K., *et al.*, 1968, *Proc. 10th Int. Conf. on Cosmic Rays, Calgary*, 1967, Vol. 2 (Ottawa: National Research Council of Canada), pp. 136–41.

Dobrotin, N. A., Grigorov, N. L., Takibaev, Zh., and Zhdanov, G. B., 1965 a, *Proc. 8th Int. Conf. on Cosmic Rays, Jaipur*, 1963, Vol. 5 (Bombay: Commercial Printing Press), pp. 141–65.

Dobrotin, N. A., *et al.*, 1965 b, *Proc. 8th Int. Conf. on Cosmic Rays, Jaipur*, 1963, Vol. 5 (Bombay: Commercial Printing Press), pp. 79–84.

Dovenko, O. I., *et al.*, 1960, *Proc. 6th Int. Conf. on Cosmic Rays, Moscow*, 1959, Vol. X (Moscow: IUPAP), pp. 134–41.

Fukui, S., 1961, *J. Phys. Soc. Japan*, **16**, 604–15.

Hasegawa, H., Noma, M., Suga, K., and Toyoda, I., 1966, *Proc. 9th Int. Conf. on Cosmic Rays, London*, 1965 (London: Institute of Physics and Physical Society), pp. 642–5.

Kameda, T., Maeda, T., Oda, H., and Sugihara, T., 1966, *Proc. 9th Int. Conf. on Cosmic Rays, London*, 1965 (London: Institute of Physics and Physical Society), pp. 681–4.

Kallmann-Bijl, H. K., *et al.*, 1961, *COSPAR Int. Ref. Atmos., CIRA* (Amsterdam: North Holland).

Kazuno, M., 1964, *Nuovo Cim.*, **34**, 303–16.

Miyake, S., *et al.*, 1966, *Proc. 9th Int. Conf. on Cosmic Rays, London*, 1965 (London: Institute of Physics and Physical Society), pp. 664–7.

Murthy, G. T., 1967, *Ph.D. Thesis*, Bombay University.

Oda, M., and Tanaka, Y., 1961, *J. Phys. Soc. Japan* (*Suppl.* A-III), **17**, 282–5.

Peters, B., 1962, *Int. Conf. on High-Energy Physics, CERN* (Geneva: IUPAP), pp. 623–32.

—— 1965, *Proc. 8th Int. Conf. on Cosmic Rays, Jaipur*, 1963, Vol. V (Bombay: Commercial Printing Press), pp. 423–42.

Tanahashi, G., 1965, *J. Phys. Soc. Japan*, **20**, 883–906.

TEUCHER, M. W., LOHRMANN, E., HASKIN, D. M., and SCHEIN, M., 1959, *Phys. Rev. Lett.*, **2,** 313.
THIELHEIM, K. O., 1964, *Nucl. Instrum. Meth.*, **31,** 341–2.
—— 1965, *Sber. Med.-Naturw. Ges. Münster (Westf.), Naturw. Abt.*, 30–9.
THIELHEIM, K. O., and KARIUS, S., 1966, *Proc. 9th. Int. Conf. on Cosmic Rays, London,* 1965 (Institute of Physics and Physical Society), pp. 779–82.
THIELHEIM, K. O., SCHLEGEL, E. K., and BEIERSDORF, R., 1968, *Proc. 10th Int. Conf. on Cosmic Rays, Calgary,* 1967, Vol. 2 (Ottawa: National Research Council of Canada), pp. 37–40.
VERNOV, S. N., *et al.*, 1960, *Proc. 6th Int. Conf. on Cosmic Rays, Moscow,* 1959, Vol. 2 (Moscow: IUPAP), pp. 115–21.
WINN, M. M., *et al.*, 1965, *Nuovo Cim.*, **36,** 701–32.